

1N 34  
2684  
P 20

# On the Anomaly of Velocity-Pressure Decoupling in Collocated Mesh Solutions

Sang-Wook Kim  
*University of Texas at Arlington*  
*Arlington, Texas*

and

Thomas VanOverbeke  
*Lewis Research Center*  
*Cleveland, Ohio*

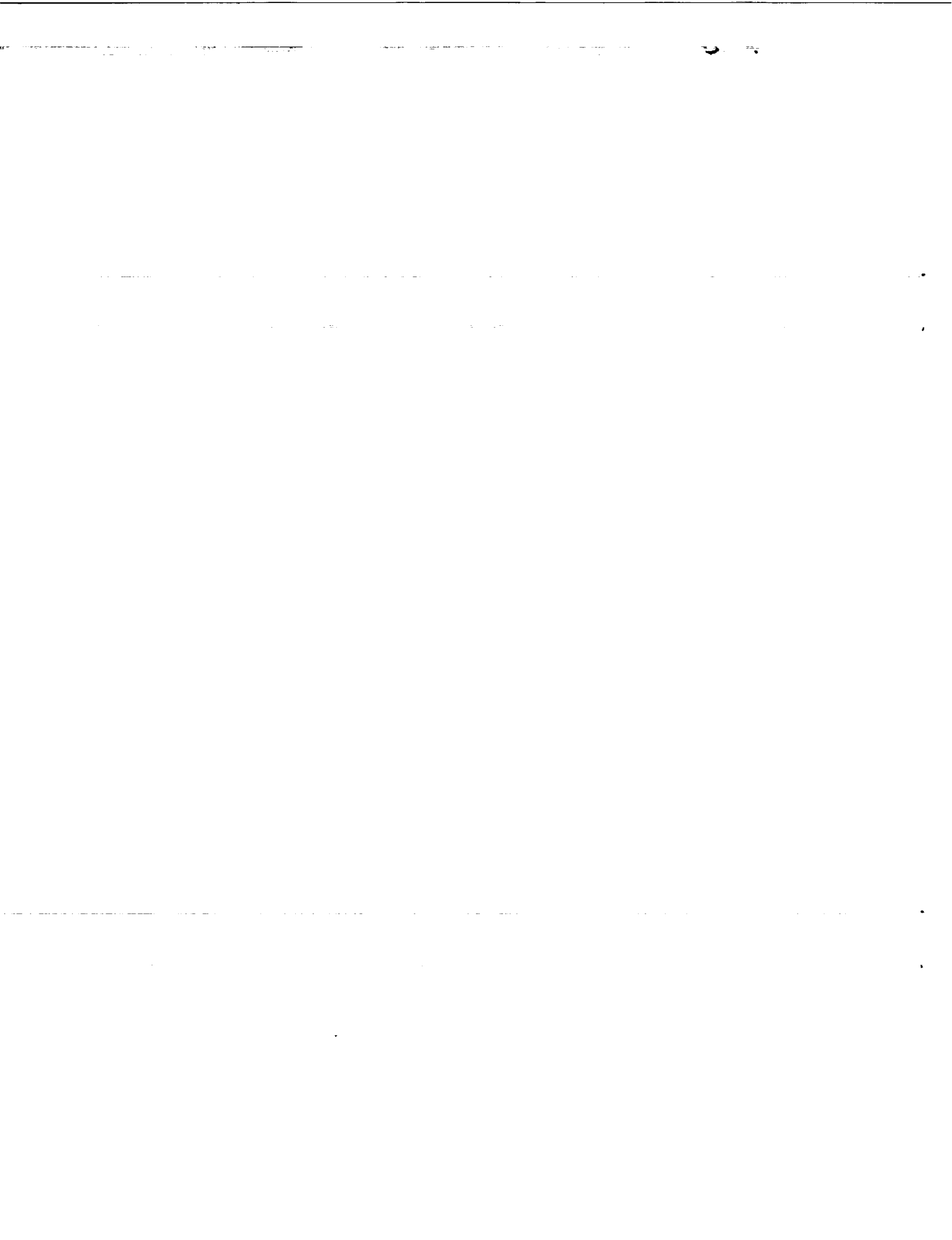
March 1991

(NASA-TM-103769) ON THE ANOMALY OF  
VELOCITY-PRESSURE DECOUPLING IN COLLOCATED  
MESH SOLUTIONS (NASA) 20 p CSCL 200

N91-21448

Unclassified  
63/34 0002684





ON THE ANOMALY OF VELOCITY-PRESSURE DECOUPLING IN COLLOCATED MESH SOLUTIONS

Sang-Wook Kim\*

University of Texas at Arlington  
Department of Aerospace Engineering  
Arlington, Texas 76010

and

Thomas VanOverbeke

National Aeronautics and Space Administration  
Lewis Research Center  
Cleveland, Ohio 44135

SUMMARY

The use of various pressure correction algorithms originally developed for fully staggered meshes can yield a velocity-pressure decoupled solution for collocated meshes. The mechanism that causes velocity-pressure decoupling is identified in this paper. It is shown that the use of a partial differential equation for the incremental pressure eliminates such a mechanism and yields a velocity-pressure coupled solution. Example flows considered are a three-dimensional lid-driven cavity flow and a laminar flow through a 90 degree bend square duct. Numerical results obtained using the collocated mesh are in good agreement with the measured data and other numerical results.

---

\*NASA Resident Research Associate at Lewis Research Center.

Nomenclature

$A_i$	coefficients for incremental velocity, ( $i=u, v, \text{ or } w$ )
$D_h$	hydraulic diameter of the curved duct
$(\ell, m, n)$	index for mesh
$n_j$	outward normal vector, $n_j=(n_x, n_y, n_z)$
$p$	pressure
$Re$	Reynolds number
$u_j$	velocity component, $u_j=(u, v, w)$
$x_j$	cartesian coordinates $x_j=(x, y, z)$
$\nu$	kinematic viscosity of fluid
$\xi_j$	curvilinear coordinates $\xi_j=(\xi, \eta, \zeta)$

Superscripts

$n$	iteration count
$nb$	neighboring grid points; $(\ell+1, m, n)$ , $(\ell-1, m, n)$ , $(\ell, m-1, n)$ , $(\ell, m+1, n)$ , $(\ell, m, n-1)$ and $(\ell, m, n+1)$
$*$	current value
$'$	incremental (or corrective) value

Subscripts

$i, j$	index for spatial coordinates, $i=\{1, 2, 3\}$ and $j=\{1, 2, 3\}$
--------	--

Mathematical symbol

$\sum$	summation
--------	-----------

## INTRODUCTION

Finite volume methods based on various pressure correction algorithms are still the most widely used numerical methods for incompressible flows. The fully staggered mesh<sup>1,2</sup> is used in most of these numerical methods to avoid velocity-pressure decoupling. However, application of the fully staggered mesh for flows with complex geometries is not straight forward, especially for three-dimensional flows. For example, the fully staggered mesh can not be used to solve flows inside a 90-degree bend duct, see Maliska and Raithby<sup>3</sup> for more details. A number of grid layouts have been proposed and are in use to solve the Navier-Stokes equations defined on complex geometries. In Maliska and Raithby<sup>3</sup>, the standard fully staggered mesh is extended in such a way that the three velocity components are located at all grid points except at the pressure grid point. In this case, the number of degrees of freedom for velocity is tripled while the degrees of freedom for pressure remains the same as that of the original fully staggered mesh. In Vanka et al.<sup>4</sup> and Chen<sup>5</sup>, the velocities are located at the same grid points and the pressure is located at the centroid of the cell formed by the four adjacent velocity grid points (for the two-dimensional case). Vanka et al.<sup>4</sup> mentioned that it was not easy to obtain convergent solutions due to velocity-pressure decoupling. This grid layout is denoted as the pressure-staggered mesh (ps-mesh) in the following discussion. In Chen<sup>5</sup>, velocity-pressure decoupling is eliminated by using a non-conforming domain for the mass imbalance calculation. A collocated mesh is used in Rhie<sup>6</sup>, Dwyer and Ibrani<sup>7</sup>, Peric et al.<sup>8</sup> and Majumdar<sup>9</sup>. In Rhie<sup>6</sup>, velocity-pressure decoupling is prevented by including a fourth order artificial dissipation in the pressure correction equation, while in Dwyer and Ibrani<sup>7</sup>, the same purpose is achieved by evaluating the incremental

velocities at mid-sides of the control volume. In Peric et al.<sup>8</sup> and Majumdar<sup>9</sup>, velocity-pressure coupling is achieved by interpolating the pressure gradient term differently from the rest of the discrete momentum equation. This interpolation scheme is called "momentum interpolation" in Majumdar<sup>9</sup>. The momentum interpolation scheme becomes similar to the present pressure correction algorithm in the case of an orthogonal mesh, and is discussed in detail in the following sections. From the above discussion, the technique for coupling the velocity and pressure forms the basis for each numerical method. In other words, the grid layout that can be used is limited by the velocity-pressure coupling mechanism to be adopted.

In the case of a collocated mesh, the velocities at odd-numbered grid points are driven by pressure at even-numbered grid points, and vice versa. Thus the momentum equation can not sense the presence of a checker-board type pressure field<sup>1</sup>. Thus it is believed that a collocated mesh yields a velocity-pressure decoupled solution. However, a number of numerical results obtained using a collocated mesh have been reported in recent years<sup>6-10</sup>. The successful calculations of various flows obtained using the collocated mesh suggest that velocity-pressure decoupling may be caused by various pressure correction algorithms rather than by the collocated mesh itself. A re-examination of the velocity-pressure decoupling mechanism in collocated mesh solutions and a partial differential equation for the incremental pressure that can be used for various grid layouts are presented in this paper.

## ANALYSIS

The incompressible laminar flow equations are given as;

$$\frac{\partial u_j}{\partial x_j} = 0. \quad (1)$$

$$\frac{\partial}{\partial x_j} (u_i u_j) - \frac{\partial}{\partial x_j} \left\{ \nu \left( \frac{\partial u_i}{\partial x_j} + \frac{\partial u_j}{\partial x_i} \right) \right\} = - \frac{1}{\rho} \frac{\partial p}{\partial x_i} \quad (2)$$

where the subscripts  $i$  and  $j$  denote each coordinate direction, and the repeated indices imply summation over the index unless otherwise stated.

In the pressure correction methods<sup>1,2</sup>, the velocities and the pressure are decomposed as;

$$u_i = u^* i + u' i, \quad (3)$$

$$p = p^* + p' \quad (4)$$

where the superscript  $*$  denotes the current velocities which may not satisfy the conservation of mass equation yet. The discrete momentum equation for  $u_i$ -velocity can be written as;

$$A_i(\ell, m, n) u_i(\ell, m, n) = \sum_{nb} \{A_i u_i\} - \frac{\partial p}{\partial x_i} + S_i^V, \text{ no sum on } i \quad (5)$$

where  $A_i$  is the coefficient of the  $u_i$ -velocity at velocity grid point  $(\ell, m, n)$ ,  $S_i^V$  is the load vector originating from the curvilinear grid structure, the superscript  $nb$  denotes the neighboring grid points, and the pressure gradient is left in continuous form deliberately. The major difference between the present pressure correction algorithm and the other algorithms originates from leaving the pressure gradient term in continuous form in deriving the pressure correction equation. In fact, velocity-pressure decoupling that occurs when various pressure correction algorithms are used for a collocated mesh or a pressure-staggered mesh is

caused by using a discretized pressure gradient in eq. (5) in deriving the pressure correction equation. The details are discussed later in this section. Substituting eqs. (3-4) into eq. (5) yields;

$$A_i(u_i^* + u_i') = \sum_{nb} (A_i(u_i^* + u_i')) - \frac{\partial(p^* + p')}{\partial x_i} + S_i^v, \text{ no sum on } i \quad (6)$$

where the grid point index ( $\ell, m, n$ ) has been deleted in eq. (6) for convenience. The discrete  $u_i$ -momentum equation based on the current flow variables which may not satisfy the conservation of mass equation can be written as;

$$A_i u_i^* = \sum_{nb} (A_i u_i^*) - \frac{\partial p^*}{\partial x_i} + S_i^v, \text{ no sum on } i \quad (7)$$

Subtracting eq. (7) from eq. (6), disregarding the summation over the neighboring grid points and the load vectors, yields;

$$u_i' = \frac{1}{A_i} \frac{\partial p'}{\partial x_i}, \text{ no sum on } i \quad (8)$$

Substituting eq. (3) into eq. (1) yields;

$$\frac{\partial u'_j}{\partial x_j} = - \frac{\partial u_j^*}{\partial x_j} \quad (9)$$

Formally substituting eq. (8) into eq. (9) yields the elliptic partial differential equation for the incremental pressure;

$$\frac{\partial}{\partial x_j} \left\{ \frac{1}{A_j} \frac{\partial p'}{\partial x_j} \right\} = - \frac{\partial u_j^*}{\partial x_j} \quad (10)$$

where the last term in eq. (10) represents the mass imbalance. Applying the standard finite volume procedure to eq. (10) yields a system of equations for the incremental pressure. In this case, the value of  $A_j$  at the interface of the pressure control volumes is obtained by linearly interpolating the adjacent nodal values. As all the central-differenced finite volume equations for self-adjoint second order elliptic partial differential equations are strongly diagonally dominant, the present discrete pressure correction equation is strongly diagonally dominant.

The mechanism that leads to a velocity-pressure decoupled solution, when various pressure correction algorithms are used for collocated or pressure-staggered meshes, is described below. In various pressure correction algorithms, the discrete pressure correction equation is obtained by integrating eq. (9) over a pressure control volume using a discretized pressure gradient in eqs. (6-8). This procedure yields a 27-diagonal system of equations for the incremental pressure for a three-dimensional case. This discrete pressure correction equation is not diagonally dominant, and thus, the mass imbalance for a particular pressure grid point tends to correct only the pressure of the adjacent pressure grid points. Velocity-pressure decoupling occurs in such a case. In case a discretized pressure gradient is used in deriving the pressure correction equation, the discrete system of equations can be made diagonally dominant by using a fully staggered mesh or by using a special interpolation scheme<sup>8,9</sup>. In the momentum interpolation scheme of Peric et al.<sup>8</sup> and Majumdar<sup>9</sup>, the pressure gradient in eq. (7) is expressed using the pressure at two grid points located across the surface of a control volume and the other terms are linearly interpolated. The discrete pressure correction

equation obtained using the momentum interpolation scheme is also strongly diagonally dominant. For an orthogonal mesh, the present pressure correction algorithm and the momentum interpolation scheme<sup>8,9</sup> yield similar seven-diagonal systems of equations for incremental pressure. The pressure correction algorithm of Peric et al.<sup>8</sup> and Majumdar<sup>9</sup> always yields a seven-diagonal system of equations for incremental pressure regardless of grid skewness, whereas, the present pressure correction algorithm yields a 27-diagonal system of equations for arbitrary skewed mesh. Through a number of numerical tests using the collocated mesh and the pressure-staggered mesh<sup>10</sup>, it was found that retaining the off-diagonal terms (which originate from the grid skewness) in the discrete pressure correction equation accelerates the convergence rate slightly compared with disregarding the off-diagonal terms. However, the advantage of slightly faster convergence rate is overshadowed by the disadvantage of the increased memory size to store the off-diagonal terms, especially for three-dimensional flows. Thus the present method and that of Peric et al.<sup>8</sup> share similar numerical characteristics. In the momentum interpolation scheme, the entire residual obtained by subtracting eq. (7) from eq. (6) is retained in eq. (8), and the residual (other than the incremental pressure gradient term) also drive the incremental pressure. Thus the numerical result may depend upon the under-relaxation parameter unless an improved momentum interpolation scheme is adopted<sup>9</sup>. On the other hand, the present method does not yield a numerical result that depends on the under-relaxation parameter as eq. (10) clearly indicates that the incremental pressure is driven only by the mass imbalance. Also the present pressure correction algorithm can be most easily extended to solve compressible flow by including convective incremental pressure terms into eq. (10), see Ref. 11 for details.

The numerical procedures are briefly described below. The pressure gradient in the momentum equation, eq. (5), for three-dimensional curvilinear coordinates, is obtained as

$$\frac{\partial p}{\partial x_i}(\ell, m, n) = \frac{\partial p}{\partial \xi_j} \frac{\partial \xi_j}{\partial x_i} \quad (11)$$

where, for example,

$$\begin{aligned} \frac{\partial p}{\partial \xi}(\ell, m, n) = & (p(\ell+1/2, m-1/2, n-1/2) + p(\ell+1/2, m+1/2, n-1/2) \\ & + p(\ell+1/2, m+1/2, n+1/2) + p(\ell+1/2, m-1/2, n+1/2))/4\Delta\xi \\ & - (p(\ell-1/2, m-1/2, n-1/2) + p(\ell-1/2, m+1/2, n-1/2) \\ & + p(\ell-1/2, m+1/2, n+1/2) + p(\ell-1/2, m-1/2, n+1/2))/4\Delta\xi \end{aligned}$$

and  $p(\ell+1/2, m+1/2, n+1/2)$  is obtained by averaging the eight adjacent nodal pressures, see Fig. 1 for the grid index. The pressure gradient equation, eq. (11), is the same as that used in the pressure-staggered mesh<sup>10</sup> and is also compatible with that proposed by Maliska and Raithby<sup>3</sup>. The same pressure gradient equation is used in evaluating the incremental velocities at the grid points, eq. (8), with the pressure in eq. (11) replaced by the incremental pressure. The power law upwind differencing scheme<sup>1</sup> is used for the momentum equation, and the discrete momentum equations and the discrete pressure correction equations are solved by the Tri-Diagonal-Matrix-Algorithm<sup>2</sup>.

#### NUMERICAL RESULTS

Numerical results for a three-dimensional lid-driven cavity flow<sup>13</sup> and

a laminar flow through a 90° bend square duct<sup>14</sup>, obtained using the collocated mesh, are presented below.

The lid-driven cavity flow at Reynolds number (based on the transverse velocity and the length of the lid) 3200 is considered. The symmetric half of the flow domain is discretized by 78x67x67 grid points in x-, y-, and z-coordinate directions, respectively. The calculated transverse and vertical velocity profiles along the center lines of the symmetry plane are shown in Figs. 2-(a) and 2-(b), respectively. It can be seen in these figures that the present numerical results compare favorably with the measured data and the other numerical results obtained by Freitas et al.<sup>15</sup> using the SIMPLE algorithm<sup>1</sup> and those obtained by Kim<sup>10</sup> using the pressure-staggered mesh<sup>10</sup>.

A laminar flow through a 90° bend square duct<sup>14</sup> is considered below. The flow geometry is schematically shown in Fig. 3. The Reynolds number based on the hydraulic diameter of the duct ( $D_h=0.04$  m) and the bulk velocity is approximately 800. The upstream boundary is located at  $10D_h$  upstream of the curved section and the exit boundary is located at  $10D_h$  downstream of the curved section. The symmetric half of the flow domain is discretized by a 92x18x33 grid points in x-, y-, and z-coordinate directions, respectively. The velocity profile of a fully developed square duct flow is prescribed at the inlet boundary and the vanishing gradient boundary condition is used at the exit boundary. The calculated longitudinal velocity profiles are shown in Fig. 4. The numerical results obtained using the collocated mesh are almost the same as those obtained using the pressure-staggered mesh. It can be seen in the figure that the present numerical results are in good agreement with the measured data and the numerical results by Humphrey et al.<sup>14</sup> The pressure distributions along

the inner and outer walls at the symmetric plane are shown in Fig. 5. The nodal pressure obtained using the collocated mesh exhibits mild wiggles. However, the averaged pressure at the cell interface varies smoothly as shown in Fig. 5. Again, the numerical results obtained using the collocated mesh are in good agreement with the other numerical results<sup>10,14</sup>. The projected velocity vectors on planes very close to the side and the bottom walls ( $0.005D_h$  away from each wall) are shown in Figs. 6-(a) and 6-(b), respectively. These planes are located so close to the wall that the velocity component normal to each plane is by far smaller than the velocity component shown in the figure. Due to the strong adverse pressure gradient, a small reversed flow region is formed near the corner wall and the reversed flow region extends up to  $\theta \approx 37^\circ$  as can be seen in these figures. The numerical results obtained using the collocated mesh are essentially identical to those obtained using the pressure-staggered mesh, see Ref. 10 for more details.

#### DISCUSSION

The use of various pressure correction algorithms<sup>1,3,4</sup> for the collocated mesh yields ill-conditioned (e.g., very small diagonal entry) discrete pressure correction equation. In such a case, the mass imbalance at a particular pressure node corrects only the pressure of the adjacent pressure grid points, and a converged solution can not be obtained. On the other hand, applying the standard finite volume numerical procedure to the partial differential equation for incremental pressure yields a strongly diagonally dominant discrete pressure correction equation and a physically consistent numerical result is obtained. The present study and those by other investigators<sup>6-10</sup> indicate that velocity-pressure decoupling is

caused by an ill-conditioned discrete pressure correction equation.

The present pressure correction algorithm and the "momentum interpolation" schemes of Peric et al.<sup>8</sup> and Majumdar<sup>9</sup> share similar numerical characteristics in the sense that these methods yield strongly diagonally dominant systems of discrete pressure correction equations. On the other hand, the present pressure correction algorithm does not involve a mixed interpolation of the discrete momentum equation as used in the momentum interpolation schemes<sup>8,9</sup>. Majumdar<sup>9</sup> pointed out that the use of a mixed interpolation for the discrete momentum equation may yield a numerical result that depends on the under-relaxation parameter and proposed an improved momentum interpolation scheme that yields a unique solution. The present pressure correction algorithm does not yield a numerical result that depends on the under-relaxation parameter, and it can also be used for pressure-staggered mesh<sup>10</sup> and compressible flows<sup>11</sup>.

#### ACKNOWLEDGEMENT

The authors would like to express their sincere thanks to Dr. Peter Sockol for many valuable suggestions for this paper.

#### REFERENCES

1. S. V. Patankar, Numerical Heat Transfer and Fluid Flow, McGraw-Hill, New York, 1980.
2. A. D. Gosman and F. J. K. Ideriah, "TEACH -T," Rept., Department of Mechanical Engineering, Imperial College, London, 1982.
3. C. R. Maliska and G. D. Raithby, "A Method for Computing Three Dimensional Flows Using Non-Orthogonal Boundary-Fitted Coordinates," International Journal for Numerical Methods in Fluids, vol. 4, pp. 519-537, 1984.
4. S. P. Vanka, B. C. J. Chen and W. T. Sha, "A Semi Implicit Calculation Procedure for Flows Described in Boundary Fitted Coordinate System," Numerical Heat Transfer, vol. 3, pp. 1-19, 1980.
5. Y.-S. Chen, "Viscous Flow Computations Using a Second-Order Upwind Differencing Scheme," AIAA Paper 88-0417, 1988.
6. C. M. Rhie, "A Pressure Based Navier-Stokes Solver Using the Multi-Grid Method," AIAA 24th Aerospace Sciences Meeting, AIAA Paper 86-0207, 1986.
7. H. A. Dwyer and S. Ibrani, "Time Accurate Solutions of the Incompressible and Three-Dimensional Navier-Stokes Equations," AIAA Paper 88-0418, 1988.
8. M Peric, R. Kessler and G. Scheurerer, "Comparison of Finite-Volume Numerical Methods with Staggered and Collocated Grids," Computers and Fluids, vol. 16, no. 4, pp. 389-403, 1988.
9. S. Majumdar, "Role of Underrelaxation in Momentum Interpolation for Calculation of Flow with Nonstaggered Grids," Numerical Heat Transfer, vol. 13, pp. 125-132, 1988.
10. S.-W. Kim, "Calculation of Separated 3-D Flows with a

Pressure-Staggered Navier-Stokes Equations Solver," NASA TM, In print, 1991.

11. S.-W. Kim, "Numerical Investigation of Separated Transonic Turbulent Flows with a Multiple-Time-Scale Turbulence Model," Numerical Heat Transfer, Part A, vol. 18, pp. 149-171, 1990.
12. S.-W. Kim, "Calculation of Reattaching Shear Layers in Divergent Channel with a Multiple-Time-Scale Turbulence Model," To appear in AIAA Journal, 1991, also available as AIAA Paper 90-0047, 1990.
13. J. R. Koseff and R. L. Street, "The Lid-Driven Cavity Flow: A Synthesis of Qualitative and Quantitative Observations," Journal of Fluid Engineering, vol. 106, pp. 390-398, 1984.
14. J. A. C. Humphrey, A. M. K. Taylor and J. H. Whitelaw, "Laminar Flow in a Square Duct of Strong Curvature," Journal of Fluid Mechanics, vol. 83, pp. 509-527, 1977.
15. C. J. Freitas, R. L. Street, A. N. Fidikakis and J. R. Koseff, "Numerical Simulation of Three-Dimensional Flow in a Cavity," International Journal for Numerical Methods in Fluids, vol. 5, pp. 561-575, 1985.

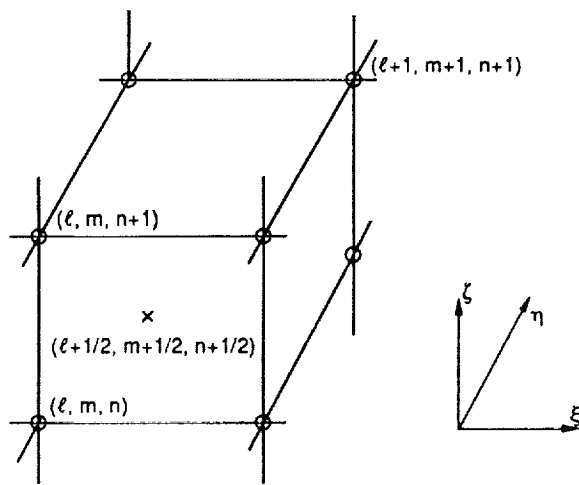
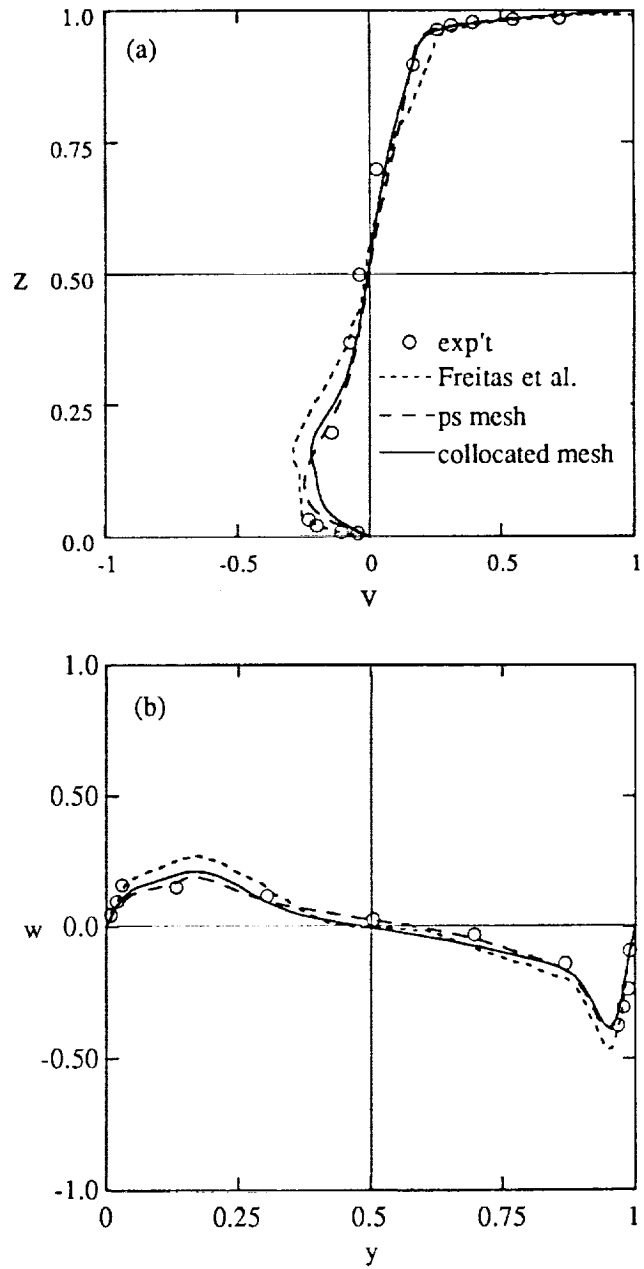


Figure 1.—Grid index for collocated mesh.



(a) Transverse velocity on symmetric plane ( $y = 0.075$  m).  
 (b) Vertical velocity on symmetric plane ( $z = 0.075$  m).

Figure 2.—Velocity profiles for cavity flow.

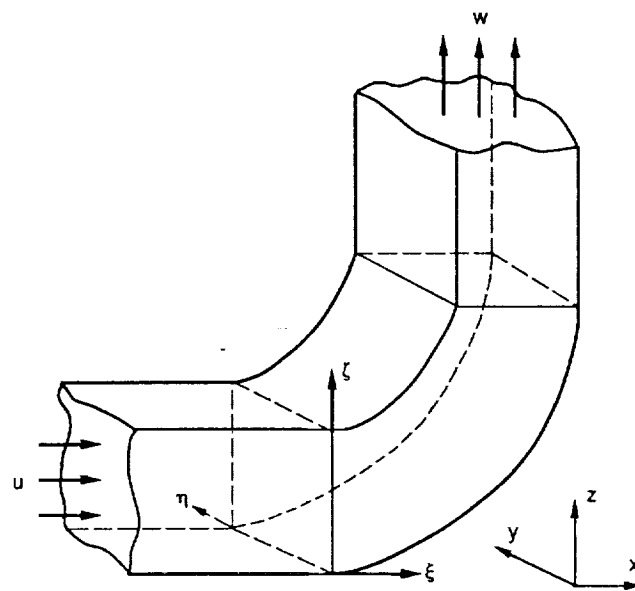


Figure 3.—Laminar flow through a 90°-bend square duct.

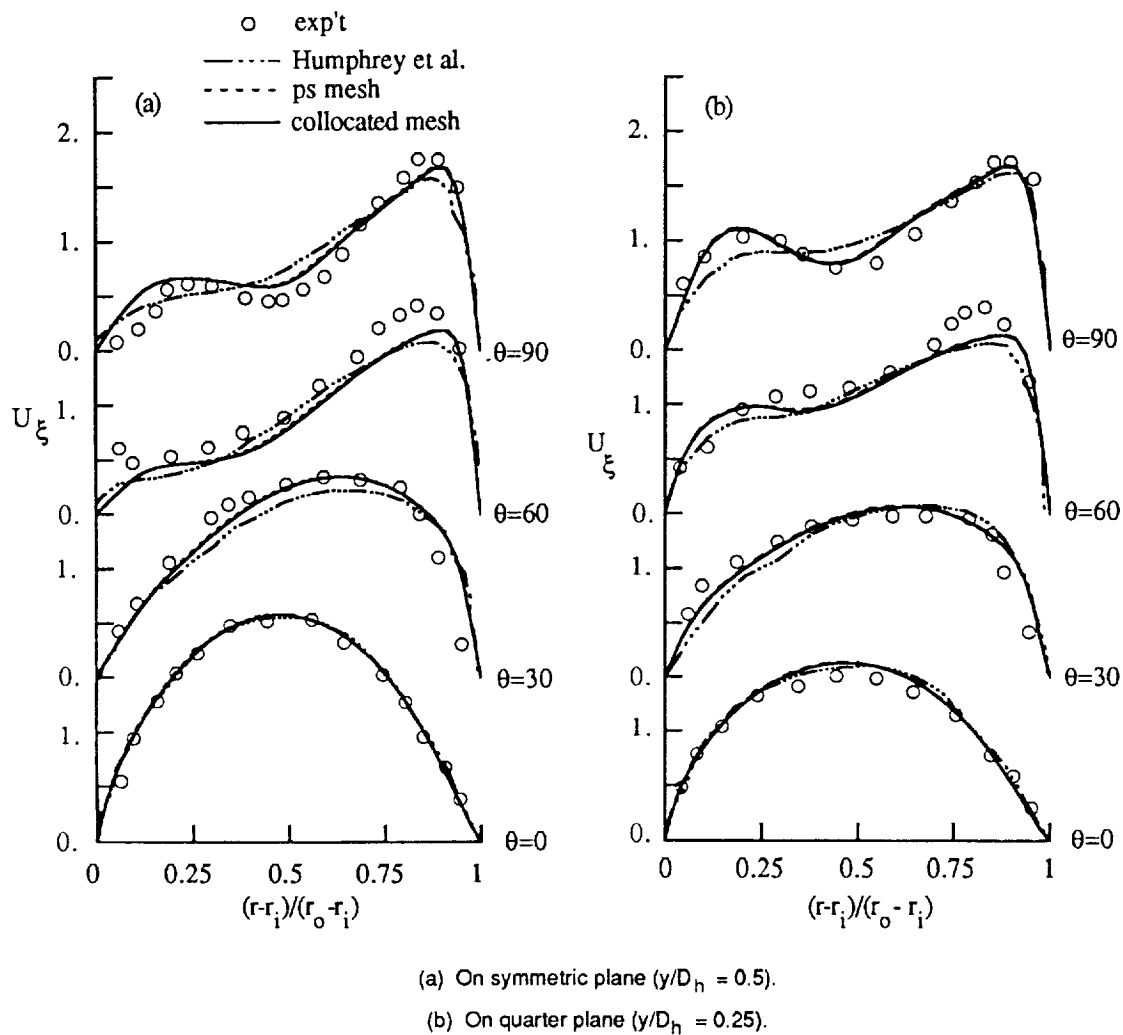


Figure 4.—Velocity profiles for curved duct flow.

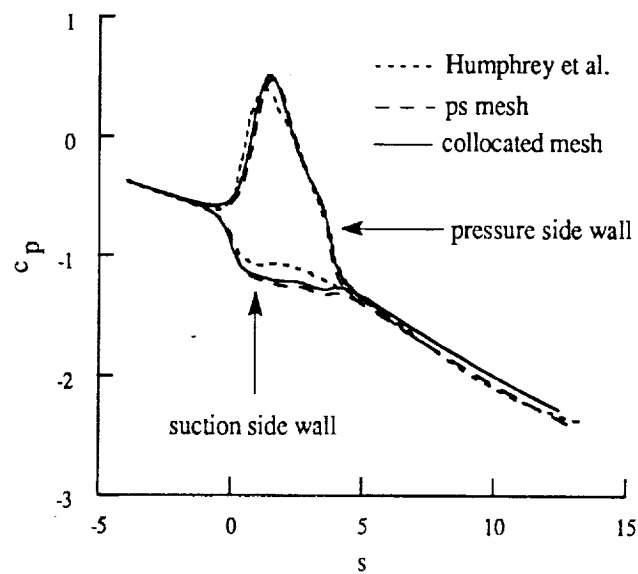
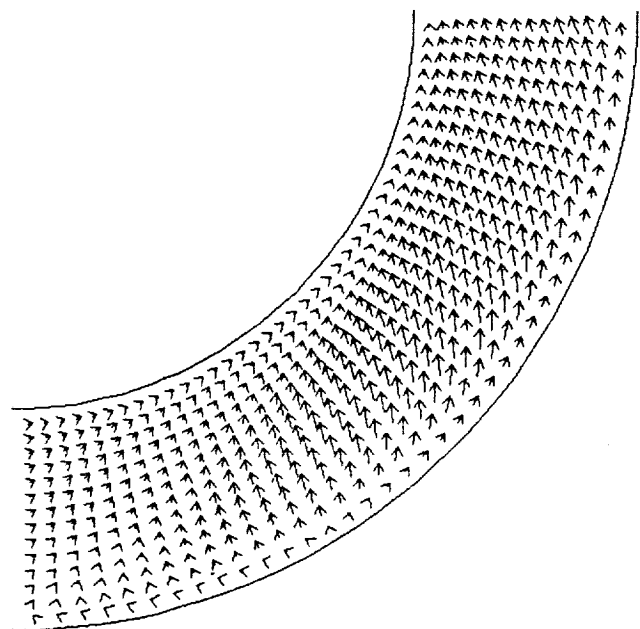
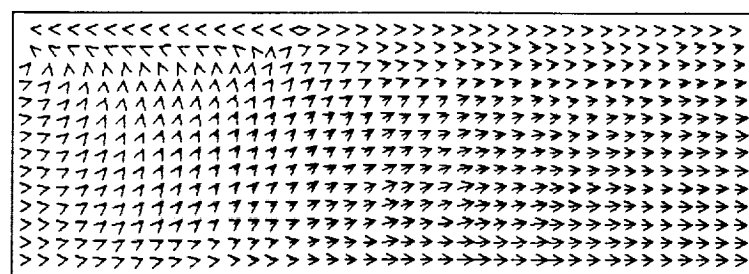


Figure 5.—Pressure distributions on the wall.



(a)  $(\xi, \xī)$  plane at  $\eta/D_h = 0.005$ .



(b)  $(\xi, \eta)$  plane at  $\xī/D_h = 0.005$ .

Figure 6.—Velocity vectors.



## Report Documentation Page

1. Report No. NASA TM-103769	2. Government Accession No.	3. Recipient's Catalog No.	
4. Title and Subtitle On the Anomaly of Velocity-Pressure Decoupling in Collocated Mesh Solutions		5. Report Date March 1991	6. Performing Organization Code
7. Author(s) Sang-Wook Kim and Thomas VanOverbeke		8. Performing Organization Report No. E - 6031	10. Work Unit No. 505 - 62 - 52
9. Performing Organization Name and Address National Aeronautics and Space Administration Lewis Research Center Cleveland, Ohio 44135 - 3191		11. Contract or Grant No.	13. Type of Report and Period Covered Technical Memorandum
12. Sponsoring Agency Name and Address National Aeronautics and Space Administration Washington, D.C. 20546 - 0001		14. Sponsoring Agency Code	
15. Supplementary Notes Sang-Wook Kim, University of Texas at Arlington, Department of Aerospace Engineering, Arlington, Texas 76010 and NASA Resident Research Associate at Lewis Research Center; Thomas VanOverbeke, NASA Lewis Research Center. Responsible person, Sang-Wook Kim, (216) 433 - 6682.			
16. Abstract The use of various pressure correction algorithms originally developed for fully staggered meshes can yield a velocity-pressure decoupled solution for collocated meshes. The mechanism that causes velocity-pressure decoupling is identified in this paper. It is shown that the use of a partial differential equation for the incremental pressure eliminates such a mechanism and yields a velocity-pressure coupled solution. Example flows considered are a three-dimensional lid-driven cavity flow and a laminar flow through a 90° bend square duct. Numerical results obtained using the collocated mesh are in good agreement with the measured data and other numerical results.			
17. Key Words (Suggested by Author(s)) Navier-Stokes equations; Cavity flow; Collocated mesh; Curved duct flow; Velocity-pressure decoupling; Incompressible flows		18. Distribution Statement Unclassified - Unlimited Subject Category 34	
19. Security Classif. (of the report) Unclassified	20. Security Classif. (of this page) Unclassified	21. No. of pages 20	22. Price* A03

